# Supporting Information

## Au@Pt NPs: Synthesis and characterization

Synthesis Route:

Au seeds

A seed-mediated approach was used to synthesize the AuPt nanoparticles, which is based on the procedure of Cignoni *et al.*[43] For the Au seed synthesis, 250 mL of ultra-pure water (ThermoFisher Scientific Barnstead Gen-Pure xCAD Plus, conductivity: ≤0.055 µS/cm at 25°C) was boiled in a 500 mL round bottom flask. 500 µL of 50 mM $HAuCl_4$ (99.99% trace metal basis Alfa Aesar) and 1250 µL 60 mM trisodium citrate dihydrate (AnalaR Normapur, VWR chemicals) were added quickly under vigorous stirring. This mixture was boiled under reflux for 1 h. After this, additional 2.5 mL of sodium citrate solution were added. Finally, the Au nanoparticle seed suspension was cooled down in an ice bath and stored in a fridge at 4 °C.

Au NPs

100 mL of ultra-pure water was cooled down in an ice bath in a 250 mL round bottom flask. 2 mL of the synthesized Au nanoparticle seeds were injected together with 500 µL of 50 mM $HAuCl_4$. Separately 4.5 mL of 100 mM L-(+)-ascorbic acid (>99 % analytical grade, Carl Roth) was cooled down in an ice bath. Once the solution was cooled down, the ascorbic acid was added dropwise using a dropping funnel within 30 min under vigorous stirring. After this the ice bath was removed and the nanoparticle suspension was stirred for further 30 min at room temperature. The suspension was centrifuged at 3000 rcf for 15 min on an Eppendorf 5810 R centrifuge. Next the supernatant was removed, and the suspension was filled up to 2 mL with ultra-pure water. The nanoparticle suspensions are stored in a fridge at 4°C.

Au@Pt

For the platinization of the Au nanoparticles, 20 mL of ultra-pure water was cooled down with an ice bath in a 100 mL round bottom flask. 1 mL of the Au nanoparticle suspension was added together with 100 µL of 10 mM $H_2PtCl_6$ (≥99.99% metal basis, Sigma-Aldrich) solution. Additionally, 240 µL of 100 mM ascorbic acid in 2 mL were separately cooled down with an ice bath. Then the pre-cooled ascorbic acid was added dropwise within roughly 30 min using a dropping funnel during vigorous stirring. After removing the ice bath and further stirring for 30 min at room temperature, the suspension was centrifuged at 3000 rcf for 15 min. Subsequently the supernatant was removed, and the suspension was filled up to 2 mL with ultra-pure water. The obtained nanoparticles were stored at 4°C in a fridge.

The synthesized Au@Pt NPs were characterized using scanning transmission electron microscopy (STEM) and energy dispersive X-ray spectroscopy (EDX). The measurements were carried out on a Jeol JEM-2800 equipped with a Schottky electron gun operated at 200 keV. Spherical and chromatic aberration are 0.7 and 1.3 mm respectively, the point-to-point resolution is 0.14 nm. EDX mapping was recorded on double SSD detectors with a spectral resolution of 133 eV. Additional characterization was done using a CPS DC24000 disc centrifuge.

STEM images (Figure S1 A) show a homogeneous distribution of Pt on the Au core, suggesting a very thin layer of Pt. Size distribution from STEM (96 NPs) show a diameter of 60 nm (Figure S1 B), the disc centrifuge measurement (Figure S1 C) suggests high agglomeration amongst the NPs (sizes > 80 nm). SEM-EDX measurements suggested a Pt content of roughly 3.5 % with 96.5 % Au.

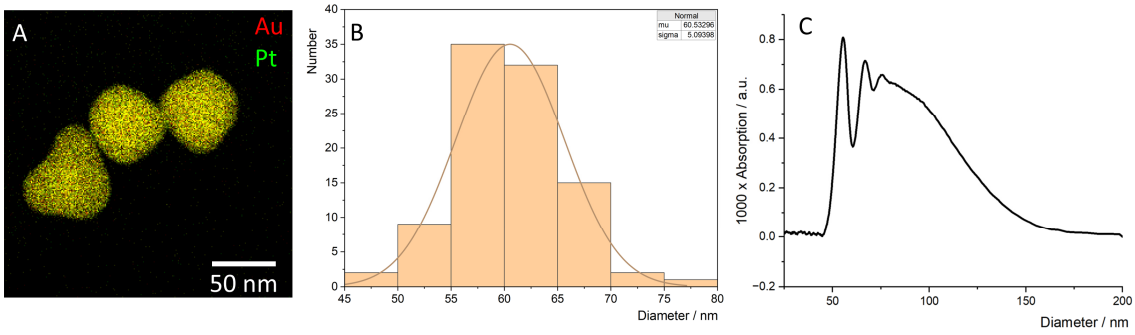


**Figure S1**: A) TEM-EDX mapping and size distribution of Au@Pt NPs determined via B) STEM and C) disc centrifuge measurements.

## Determination of Experimental Parameters

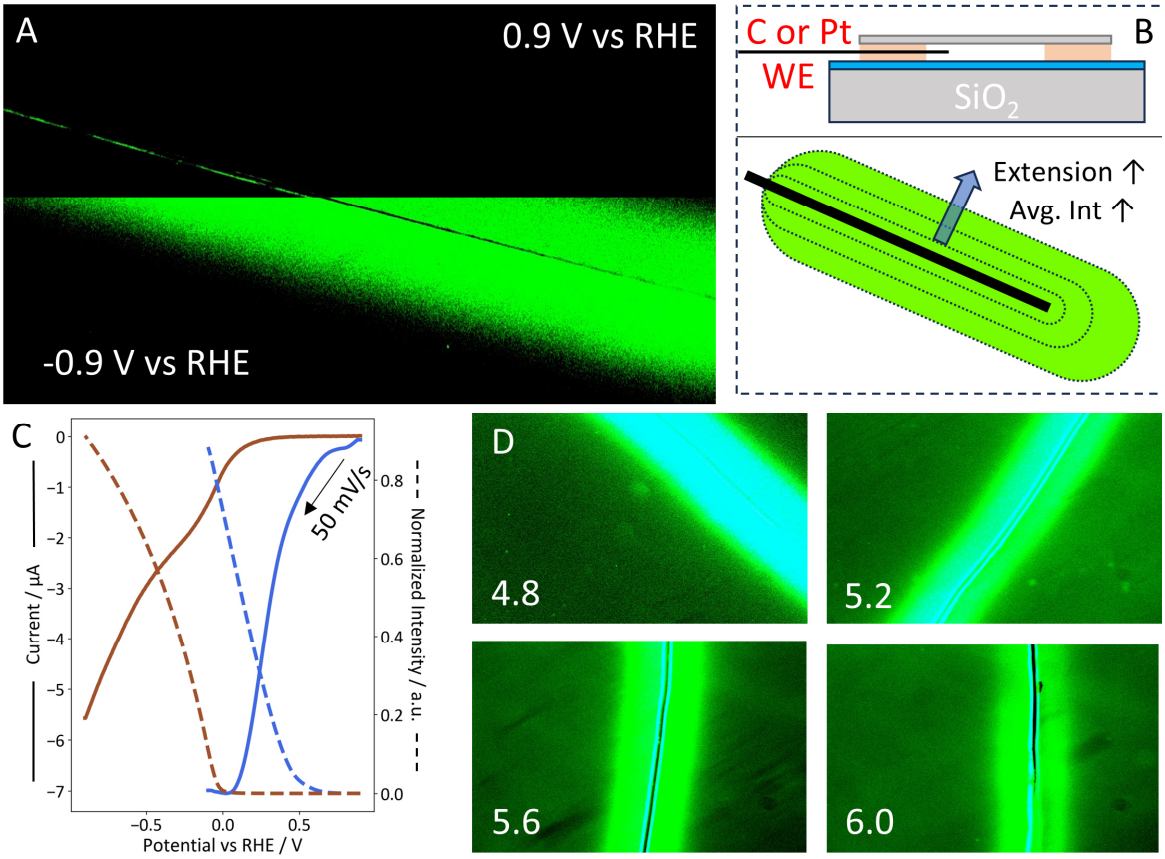


**Figure S2:** A) Carbon-fiber electrode at 0.9 V and −0.9 V vs RHE which was recorded during a LSV with a scan rate of 50 mV/s. B) Experimental setup and working principle of the measurement: With progression of the experiment, the growth of the fluorescent layer corresponds to an average intensity increase of the respective frames, yielding an optical LSV. C) Comparison of optical and electrochemical LSVs recorded at C-fiber (brown) Pt-wire (blue), the average G-channel intensities are shown as dashed line, the current is presented as solid line. D) Pt-wire electrodes during 5 s potential pulses at 0.1 V vs RHE in fluorescein containing electrolyte with different pH values, as specified in the bottom left corners of the images. The displayed images were recorded at 60 % of the pulse duration. All CCD videos were recorded with an exposure time of 50 ms, a blue LED as widefield illumination source and a 520 nm emission filter.

As a sample with low catalytic activity, a carbon-fiber (carbon-fibers were purchased from Goodfellow Cambridge Ltd.) was used as WE in a thin-layer setup (compare Figure S2 A and B) and an LSV was recorded from 0.9 to −0.9 V vs RHE (50 mV/s, pH of electrolyte was adjusted to 4.8). Figure S2 A shows the fiber at the start (top half) and the end (bottom half) of the measurement, where the emerged fluorescent region can clearly be distinguished from the dark background. We introduce the term “directed fluorescence” to describe the situation in which a clear origin of the fluorescent region (i.e. the wire) can be observed, as opposed to “substrate fluorescence”, where a homogeneous fluorescence emerges throughout the monitored region. From the recorded CCD video, the averaged G-channel intensity was extracted and plotted vs the applied potential to obtain an optical LSV. The G-channel was herein chosen due to the green emission of fluorescein which should provide the highest intensity amongst the RGB channels of the CCD camera. The plot in Figure S2 C (brown color) shows the obtained electrochemical and optical CV with an onset potential of approximately −0.1 V vs RHE which we herein define as the potential where 5 % of the maximum

fluorescence intensity is reached (maximum intensity was reached after the measurement finished).

As a catalytically very active material, a Pt wire (Pt wires, 25 µm diameter, were purchased from Ferro GmbH) was used as WE under similar conditions, yielding the optical LSV shown in Figure S2 C (blue color). Here, the onset potential was found to be roughly 0.5 V more anodic than it was the case for the C-fiber which indicates the higher catalytic activity of Pt compared to C (see Figure S2 C brown color).

To ensure high sensitivity to small pH changes, a pH high enough to be close to the equivalent pH of fluorescein (with a $pK_A$ of roughly 6.5 for dianionic species) but low enough to ensure a good fluorescence intensity to background intensity ratio was crucial for the experiments. To determine a suitable pH value for our experiments, different identical electrolyte solutions were prepared and adjusted to pH values of 4.8, 5.2, 5.6 and 6.0. The appearance of the directed fluorescence was then studied by applying 5 s pulses at 0.1 V vs RHE, which according to Figure S2 C is sufficiently cathodic to provide a significant fluorescence response. The image intensity threshold was adjusted to provide comparable background intensities. As the fluorescent background was already strong for the electrolytes above pH 5.2, the resulting fluorescence signal for these experiments was comparably weak, as shown in Figure S2 D. One should note that no significant difference in the extension of the fluorescent region was observed. According to Figure S2 D, pH values between 4.8 and 5.2 provide sufficient fluorescence in comparison to the background. Therefore, we conducted the experiments with electrolytes adjusted to a pH value of 5.1.

Apart from the initial pH value, also the dye concentration affects the behavior of the fluorescence response, as fluorescein itself acts as buffer to the system and may therefore attenuate the effect of proton depletion. Different fluorescein concentrations in the range from 20 µM to 600 µM were tested with the same experimental configuration involving a Pt WE, as for the pH optimization (Figure S2). The pH was adjusted to 5.1 and 125 mM $K_2SO_4$ was used as supporting electrolyte. CCD videos were recorded during consecutive pulses of 0.9 V and 0.4 V vs RHE, which is sufficient to produce a fluorescent layer at the Pt WE according to Figure S2 D). A detailed description of the data extraction is given in S3.

Figure S3 shows the buffering effect of the fluorescein, where the propagation speed of the fluorescent region and thus of the diffusion layer of proton depletion is a function of the dye concentration. While the fluorescent layer extends far into the solution at low fluorescein concentrations, a very thin fluorescent layer is found at high fluorescein concentrations. Although the trend shown in Figure S3 implies a higher sensitivity to slight pH changes near the electrode surface with lower dye concentration, the drawback of the dye dilution is the overall lower fluorescence intensity, making the

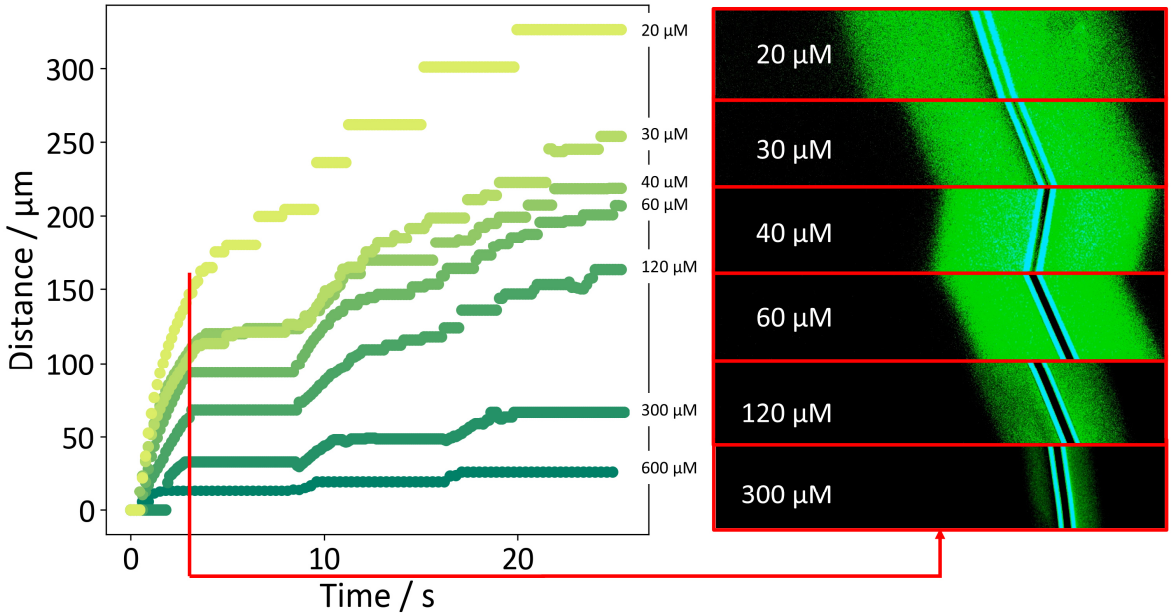


**Figure S3**: Development of the fluorescent front during subsequent potential pulses (2 s at 0.9, 5 s at 0.4 V vs RHE, 3 repetitions). The red vertical line marks the time at which the respective images shown on the right were recorded. Different concentrations of fluorescein solutions were used, the pH was adjusted to 5.1 and 125 mM $K_2SO_4$ was the supporting electrolyte.

distinction between directed fluorescence and substrate fluorescence signal more difficult for higher dilutions. This can be seen as decrease in the fluorescence intensity for concentrations lower than 40 µM.

To generate a reference for the fluorescent layer distance determination, the first frame of the video was converted to grayscale and pixels above an arbitrarily chosen threshold were set to maximum intensity (white), whereas pixels with lower intensity were set to zero intensity (black). The white pixels were predominantly located at the bright positions of the Pt-wire. Coordinates of the white pixels were extracted, and a linear fit was applied to these coordinates. This initial reference line is indicated as red line in the scheme below.

For the distance determination of the fluorescent layer, grayscale difference frames were calculated (Difference = Frame N – Frame N-1; N represents the frame index) for each frame in the video with N > 1. Setting pixel values where the difference is larger than an arbitrarily defined threshold to maximum intensity provided binary images. Herein white pixels represent a sufficient change in intensity and black pixels represent no change. The positions where the thus calculated binary difference images contain white pixels were then extracted and used for a linear fit (green line in scheme below).

The linear fit of the difference frames was adjusted so that the slope equals the slope of the wire linear fit and the distance between the parallel lines was then calculated for each frame. Including the scaling factor of the microscope to convert pixel distances into micrometer scale and the used exposure time for converting frame numbers into time coordinates, the plots shown in Figure S3 were obtained.

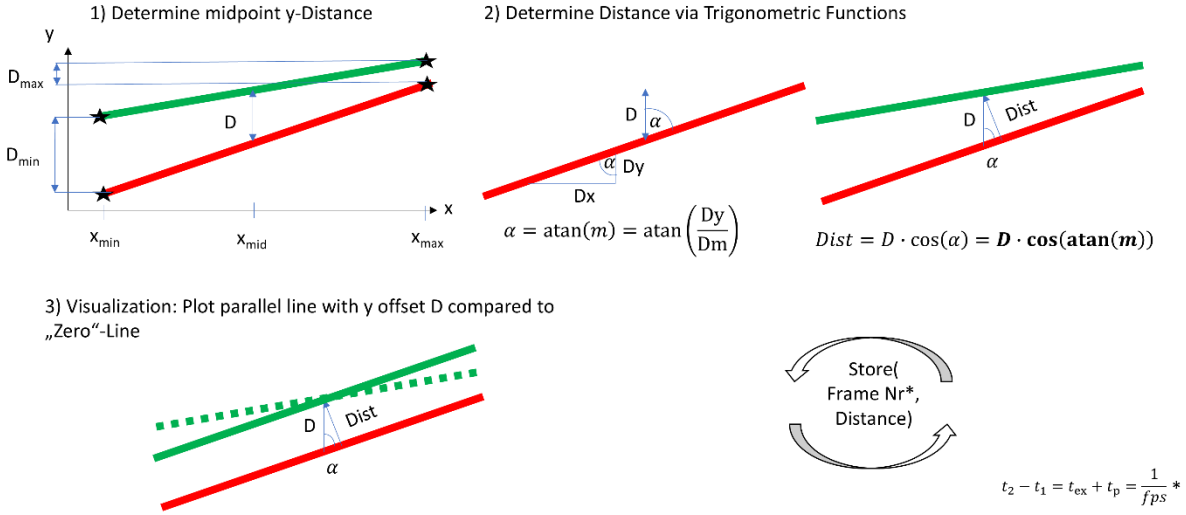


**Figure S4**: Schematical representation of the distance determination loop used to extract the datapoints shown in Figure S3.

## Fluorescence spectra of unmodified ITO

The following figure was made from the same dataset as shown in Figure S2. Unlike the figure shown in Figure S2, this spectral time series was extracted from a spot where no Au@Pt NP was present. By comparing Figure S5 to Figure S2 it becomes clear that the only difference is the absence of the LSPR band in Figure S5. Thus, it can be concluded that the fluorescence response is independent of the presence of single NPs and just represents the ITO substrate fluorescence.

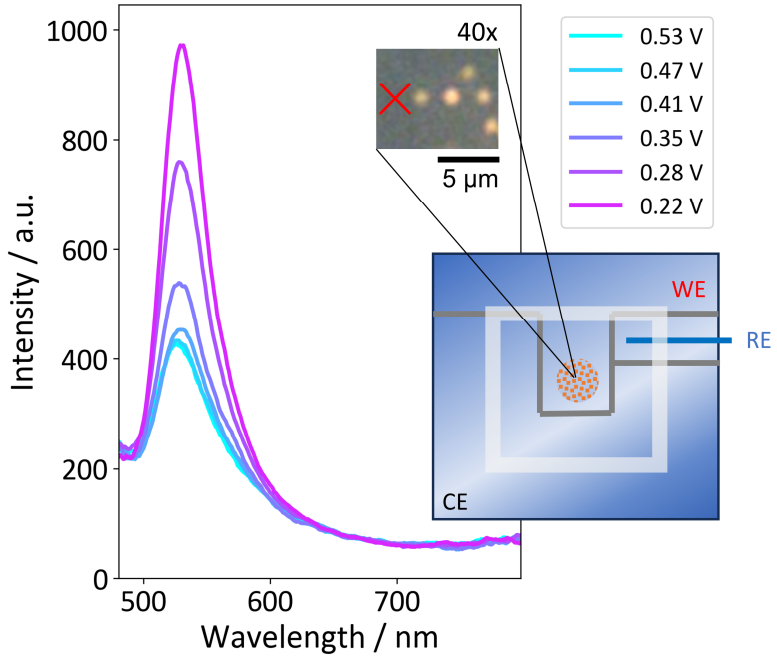


**Figure S5**: The same spectral time series shown in Figure 2, but at a position without NP, as indicated by the red cross in the inset image. The potentials correspond to an RHE. The schematic cell design is shown as an overlay, indicating the positions of the NPs on the ITO substrate.

## Videos

Figure 2 a) was created from the videos

S7-1: Untreated ITO surface during reductive LSV (0.9 V to 0.1 V vs RHE, 5 mV/s)

S7-2: Au@Pt nanoparticle-modified ITO during reductive LSV (0.9 V to 0.1 V vs RHE, 5 mV/s)

Figure 3 was created from the videos

S7-3: 300 ms pulses at 0.0 V vs RHE. Including the aggregate of Figure 3B

S7-4: 300 ms pulses at 0.0 V vs RHE. Including the aggregate of Figure 3A